A MEMS VOA Using Electrothermal Actuators

Chengkuo Lee, *Member, IEEE*

***Abstract*—A comprehensive study of electrothermally driven microelectromechanical system (MEMS) variable optical attenuator (VOA) devices using an H-shaped structure is presented in this paper. Based on its unique structural design, a retroreflection-type VOA of smaller footprint is realized. The repeatability and stability of the static and transient characteristics of attenuation behavior at various ambient temperatures are characterized. The fluctuation of attenuation curves under the same driving voltage at the same ambient temperatures is less than $\pm$0.1 dB. Again, comparing the attenuation curves measured at 25 °C to 75 °C and at 25 °C to 12.5 °C, the deviation of attenuation under the same driving voltage is within the 0.6-dB range. Within the 40-dB attenuation range, the measured switching time from nonattenuation state to a particular attenuation state or between two attenuation states is less than 10 ms. This electrothermally actuated MEMS VOA also demonstrates the state-of-the-art dynamic attenuation stability that complies with the Telecordia GR1221 regulations, where the dynamic fluctuation of attenuation at 20 dB is less than $\pm$0.36 dB under a vibration testing condition of 20 G periodical shocks with frequency from 20 Hz to 2 kHz.**

***Index Terms*—Electrothermal actuators, microelectromechanical systems (MEMS), reliability, telecordia, variable optical attenuators (VOAs), wavelength division multiplexing.**

I. Introduction

MICROELECTROMECHANICAL system (MEMS)-based technologies and solutions have been successfully applied to various tunable devices in the optical network. Since the MEMS-based components normally provide advantages over other solutions in terms of device features of wavelength independence, protocol and bit rate independence, etc., various MEMS devices for optical communication components have been demonstrated up to date. These devices comprise low port count optical switch, planar two-dimensional (2-D) optical switch, three-dimensional (3-D) optical switch, single-channel variable optical attenuators (VOAs), multichannel VOA, dynamic gain equalizer, and so on [1]–[3]. With the aforementioned advantages, MEMS VOA is a kind of fundamental tunable component with the function of controlling the propagated level of light power. VOA provides gain equalization in optical amplifiers, channel blanking for network monitoring, and signal attenuation to prevent detector saturation [4]–[6], [10]. For example, in wavelength-division multiplexing systems, a spectrally flat signal is preferred to reach a state where all of the channels have substantially the same gain. Therefore, such a kind of signal can be transmitted for a longer distance without regeneration while still permitting the constituent channels to be distinguished from one another by a receiver.

Various types of VOAs that use different MEMS mechanisms and light path designs to form diversified light attenuation configurations have been proposed. These VOAs can be categorized into two groups in terms of their difference in spatial arrangement of all elements regarding light path, namely 1) the planar VOA and 2) the 3-D VOA. The difference in optics and spatial arrangement of all the elements will also lead to a choice of appropriate MEMS actuators. Two major groups of MEMS actuators have been applied to conceptualize VOA devices. They are electrostatic actuators, e.g., surface micromachined parallel plates [4]–[9], bulk micromachined comb drives [10]–[17], and rotary comb drives [18], [19], and electrothermal actuators, e.g., U-shaped actuators [20], [21], V-beam actuators [22], [23], and H-shaped actuators [24]. Generally speaking, electrostatic actuators have been the dominant solutions for driving MEMS VOA. Since there is no current flowing between the electrodes of electrostatic actuators, it means no power consumption within the actuator part in the operation of electrostatic actuators. On the other hand, the electrothermal actuators have been known for their large displacement and high force output. These characteristics make electrothermal actuators an alternative for the VOA device. The size and weight of MEMS elements are relatively small, i.e., only a small energy is required to operate the MEMS-based VOA. In other words, the power consumption of electrothermally driven MEMS VOA is expected to be low as well. Second, the nature of the electrothermal actuator structure renders electrothermally driven MEMS VOAs with a smaller footprint and lighter weight than their counterpart based on electrostatic actuators. Such characteristics could let us make multichannel VOAs that are much smaller, in contrast to previous electrostatically driven MEMS multichanneled VOAs [25], [26].

The promising dynamic attenuation feature of H-shaped MEMS VOA that has been highlighted in [24] inspires the author to do a more extensive study. Moreover, it is suspicious that the ambient temperature will influence the heat dissipation rate of electrothermal actuators. Such an ambient temperature variation effect may cause a potential difference of actuated light beam path with regard to the same electrothermal actuator under the same driving condition. Thus, the behavior and performance of H-shaped MEMS VOAs under ambient environments with large temperature variation are investigated in this paper.

Manuscript received March 27, 2006; revised October 9, 2006. This work was supported in part by grants from a joint-funded research project based on Faculty Research Fund R-263-000-358-112/133 of the National University of Singapore and from the Institute of Microelectronics, A*STAR, Singapore.

The author is with the Department of Electrical and Computer Engineering, National University of Singapore, Singapore 117576, and also with the Institute of Microelectronics, A*STAR, Singapore 117685 (e-mail: elelc@nus.edu.sg; leeck@ime.a-star.edu.sg).

Color versions of one or more of the figures in this paper are available online at http://ieeexplore.ieee.org.

Digital Object Identifier 10.1109/JLT.2006.888257

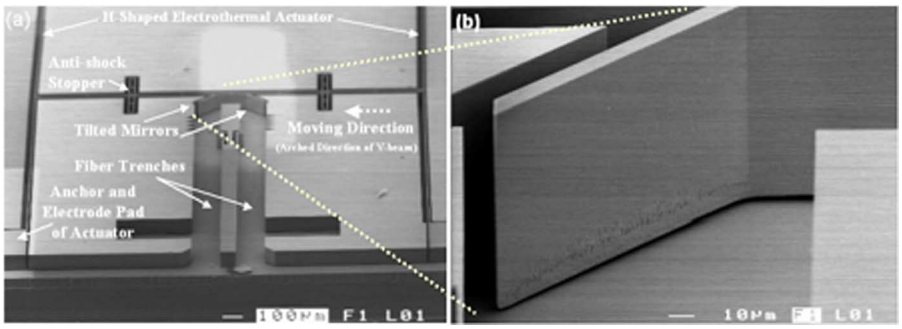

Fig. 1. (a) SEM photograph of a MEMS VOA device comprising a pair of tilted mirrors driven by an H-shaped electrothermal actuator, where four anchors of actuator are symmetrically allocated on four corners. (b) SEM photograph of the closed-up view of a tilted mirror.

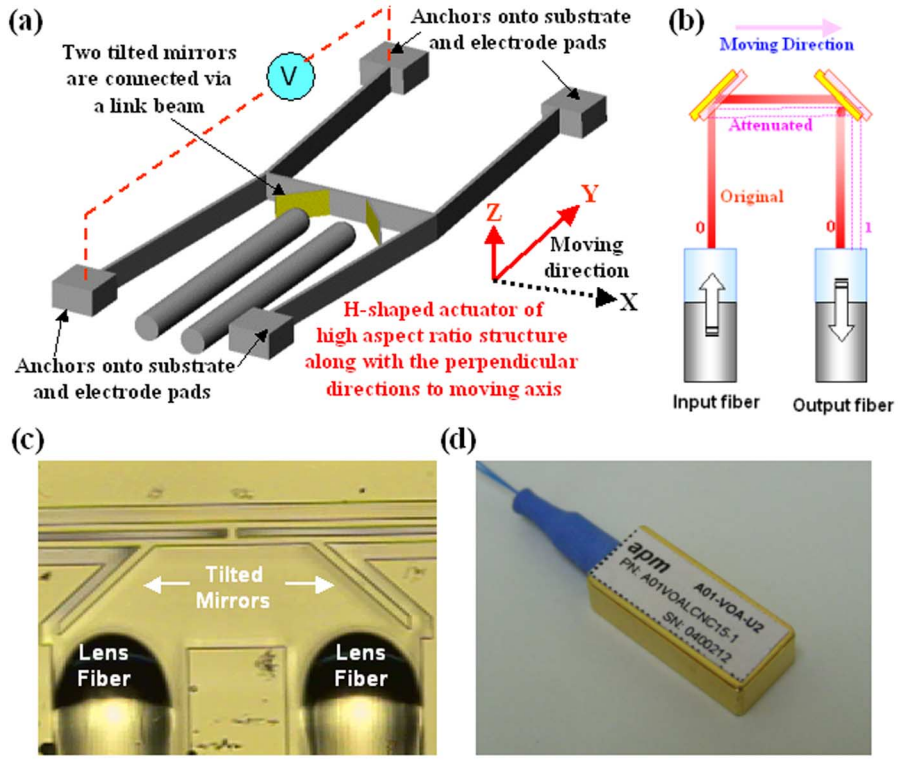

Fig. 2. (a) Schematic drawing of the H-shaped beam structure of an electrothermal MEMS VOA. (b) Schematic drawing of the attenuation of retroreflection light path misalignment, where the attenuated light path 1 is deviated from the optimized coupling path 0 pertinent to the original rest state of nonattenuation. (c) Optical micrograph of the pair of tilted mirrors and two coaxially arranged lens fibers. (d) Photo of a packaged MEMS VOA device.

II. Micromechanism and Attenuation Characteristics

The VOA devices were made by using deep reactive ion etching (DRIE) to pattern the H-shaped structures from the device layer with 82 μm of a 6-in silicon-on-insulator (SOI) wafer. After the DRIE step, the thermal oxide layer underneath the H-shaped structure from the device layer of the SOI wafer was removed by wet etch in a hydrofluoric-acid-buffered solution. Only the thermal oxide layer underneath the anchors was kept there without being fully etched away. A single chip made from the H-shaped structure is shown in Fig. 1(a). Fig. 1(b) shows a close-up view of the left-hand-side-tilted mirror. The electrical pads are the anchors that are made of Si, as shown in the left bottom corner of Fig. 1(a). Having a smooth mirror surface with sub-micrometer scale flatness is crucial to the good optical characteristics. After separation, the known good die characterization has been done by an examination in mirror displacement under electrical dc biases via a charge-coupled device (CCD) camera. The selected good dies with qualified motion characteristics of mirrors were moved to and fixed on a precision XYZ stage. Two lens fibers were placed in two parallel trenches and faced toward tilted mirrors in front of themselves, as shown in Fig. 2(a) and (c). These lens fibers are commercially available components: the same as the ones used in [27]. The details of specifications of this sort of lens fiber are discussed in [27]. These two mirrors with 45° tilted angle arranged face to face at the center of the link beam can enable a retroreflection light path regarding the input light path and the twice-reflected light path. First of all, a 1550-nm laser was fed into the input lens fiber, and the initial insertion loss was measured while we moved and rotated these two lens fibers in

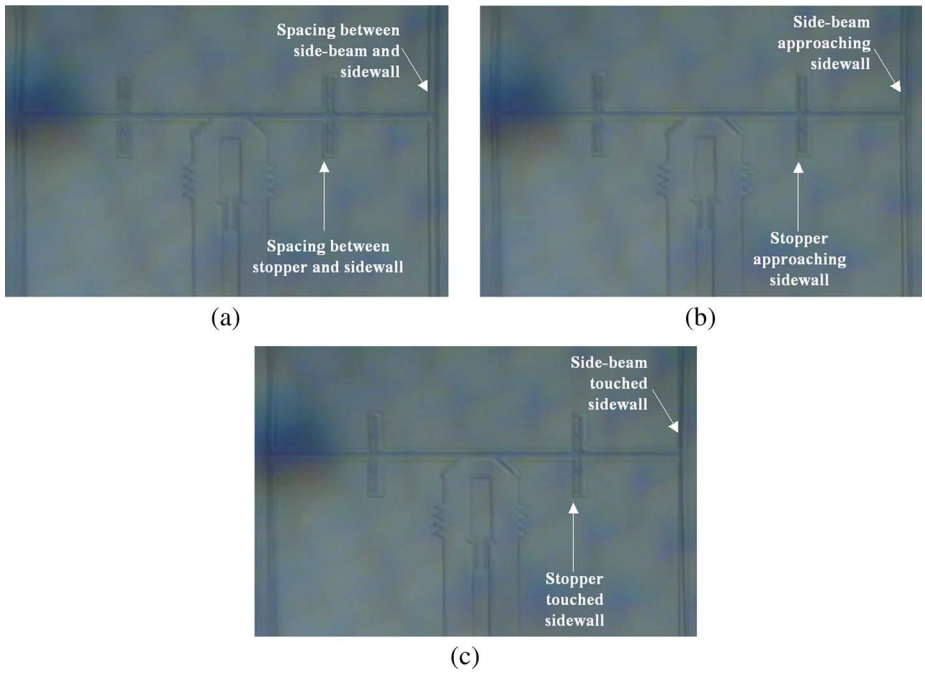

Fig. 3. CCD images of the H-shaped beam structure of MEMS VOA device. (a) CCD image of the H-shaped beam structure in the rest state of nonattenuation. (b) CCD image of the H-shaped beam structure in its attenuation state under a dc voltage where it is bent to drive the pair of tilted mirrors moving toward the left-hand side. (c) CCD image of the H-shaped beam structure in a state where anti-shock stoppers driven by the bent H-shaped beam structure encounter the left sidewall due to an overshot voltage.

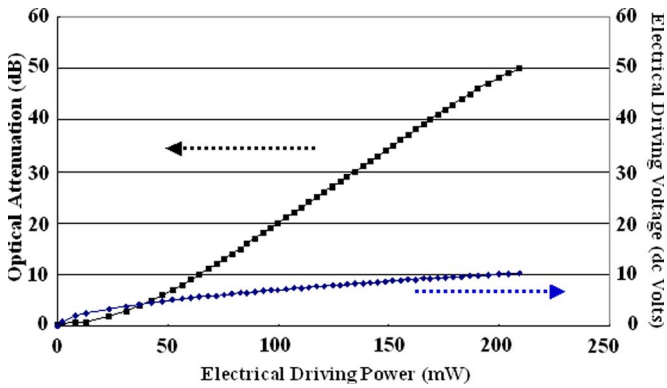

Fig. 4. Curves of measured attenuation versus driving voltage and electrical power.

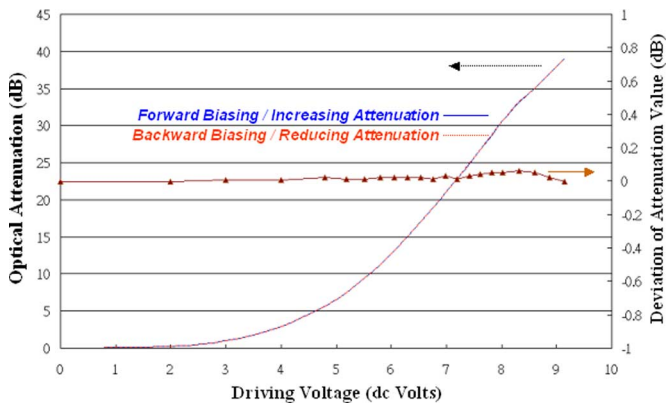

Fig. 5. Measured attenuation curves and curve of deviation values within a cycle of attenuation operation between its zero attenuation and 40-dB attenuation.

order to reach minimum insertion loss, which is typically less than 0.8 dB. Second, as shown in Fig. 2(a) and (b), we applied dc voltage on the anchors of both sides of the H-shaped beam structure to generate a net displacement due to the joule-heated volume expansion caused by the electrical current flowing via the said beam structures. The moving direction is the arched direction of side beams toward the right side. This moving axis is defined as x-axis. Thus, the net displacement along the x-axis depends on the applied voltage. When both reflective mirrors moved toward the right side, the second reflection light path, denoted as path 1 in Fig. 2(b), was deviated from the original optimized path of the state reaching the minimum insertion loss, i.e., path 0 in Fig. 2(b). Therefore, the coupled reflected light intensity toward the output port was reduced. Attenuation was performed by controlling the deviated distance between the second reflected path with respect to various applied dc biases and path 0. When the applied voltage is removed, both mirrors will return to their rest position, and the light path will become path 0 again. The attenuation curve versus driving voltage was derived first, and then, the polarization-dependent loss (PDL) was measured with regard to the particular attenuation values. Samples with PDL of less than 0.4 dB within 30-dB attenuation were selected as qualified dies for the next packaging step. Fig. 2(d) shows a packaged MEMS VOA device with size $12.5 \times 6.8 \times 3.5$ mm (length, width, and height).

TABLE I
MEASURED PDL, WDL, AND RETURN LOSS VERSUS ATTENUATION

Attenuation	0dB	3dB	10dB	20dB	30dB
Measured PDL (dB)	0.05~0.08	0.07~0.10	0.10~0.18	0.20~0.27	0.21~0.39
Measured WDL (dB)	0.04~0.09	0.06~0.15	0.15~0.28	0.30~0.45	0.40~0.65
Measured Return Loss (dB)	51~52	51~52	50~52	50~52	50~52

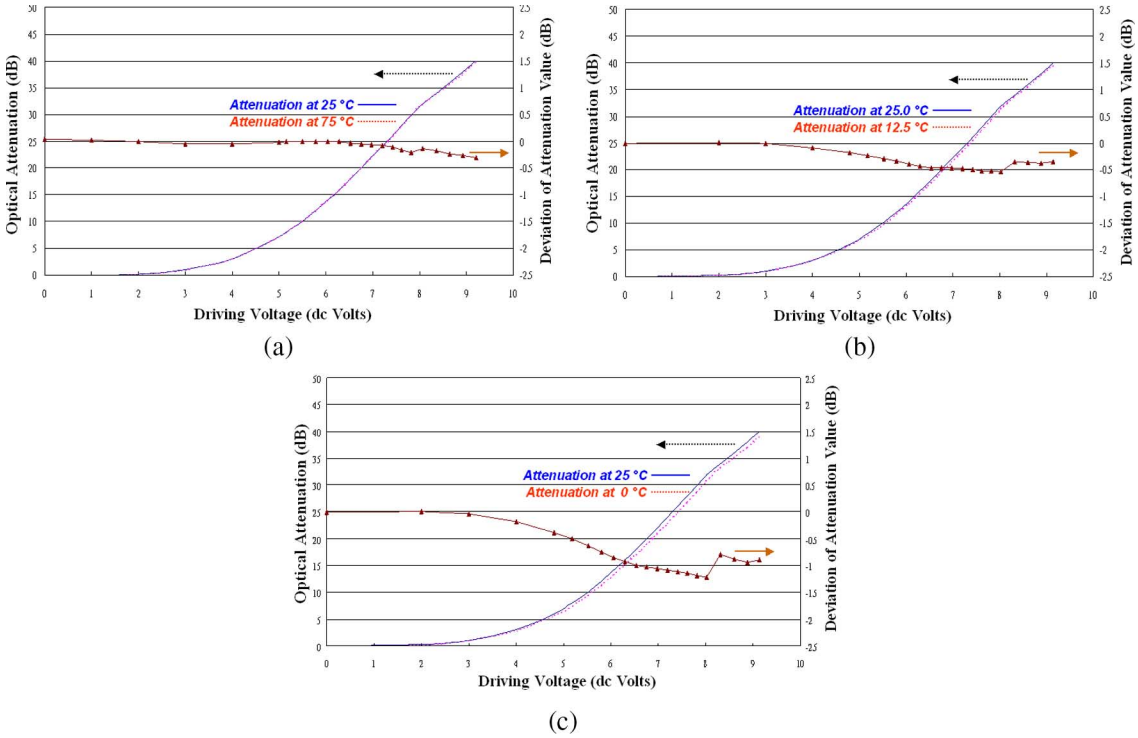

Fig. 6. Attenuation curves measured at two temperatures and curve of deviation values with regard to these two attenuation curves. (a) 25 °C versus 75 °C. (b) 25 °C versus 12.5 °C. (c) 25 °C versus 0 °C.

On the other hand, Fig. 3(a) shows the CCD image of the initial state of the H-shaped structure, i.e., nonbiasing state. Fig. 3(b) to (c) displays the sequentially caught CCD images pertinent to the moving process of two tilted mirrors driven by deflected side beams of the H-shaped structure under dc voltage of about 15 and 22 V, respectively. Comparing Fig. 3(b) with Fig. 3(a), we could observe that the deformed side beams of the H-shaped structure provide mirror displacement toward the left side, and the stopper is almost approaching the silicon sidewall. Moreover, Fig. 3(c) shows that the stopper structure and the deformed side beams touched the left sidewall, when the applied voltage was much larger than necessary, such as 22 V. This stopper concept was also used as the structural anti-shock protection against unwanted mechanical impact or environmental shock, e.g., dropping down to floor. In fact, only 10.2 V dc is required for 50-dB attenuation, as shown in Fig. 4. This implies that the mirror displacement responsible for 30 dB is much less than what we observed in Fig. 3(b), while 30-dB attenuation is normally considered as the upper bound of operation of attenuator devices for most industrial applications. The upper curve in Fig. 4 represents the characteristics between attenuation and electrical driving power. The relationship between driving power and driving voltage is characterized by a linear line at the bottom of Fig. 4. It points out that only 135 mW was required to maintain the device operating at 30-dB attenuation. A driving power of 210 mW can maintain the VOA device at 50-dB attenuation state.

In order to further confirm whether there is hysteresis effect on the optical attenuation versus electrical voltage curve, the attenuation versus driving voltages in forward/backward biasing steps was measured at 25 °C, as shown in Fig. 5. Due to the scale, the attenuation curves of forward/backward biasing coincide and look like a single curve instead. It reveals that the difference between forward-biased and backward-biased attenuation values under the same driving voltage is less than ±0.1 dB within the full span of the 40-dB attenuation range. The data curves measured at 0 °C and 75 °C were of the same quality as the one shown in Fig. 5. It also implies that there is no such hysteresis issue to be concerned for electrothermally driven MEMS VOAs.

Besides, PDL, wavelength-dependent loss (WDL across the full C- and L-bands), and return loss are characterized within the 30-dB attenuation range. These optically related device features are mainly correlated with the light path design of attenuation, size, and flatness of mirrors and optics. Since the same microfabrication procedure and retroreflection light path scheme for attenuation are adopted in this paper, the data shown in Table I reveal the same level of quality as the data discussed in previous works [15], [25], [26]. Briefly speaking, the return loss is better than 50 dB within the 30-dB attenuation region. For a large portion of the samples, PDL and WDL are less than 0.3 and 0.55 dB within the 30-dB attenuation region, respectively.

III. Dynamic Characteristics of MEMS

On the other hand, we had reported the design and performance of using various types of electrothermal actuators for optical switches [28], [29]. In contrast to the ON–OFF states of operation required for the optical switch, the dynamic characteristics and the stability of the mirror driven by electrothermal actuators at any transient point of a continuous actuated trace

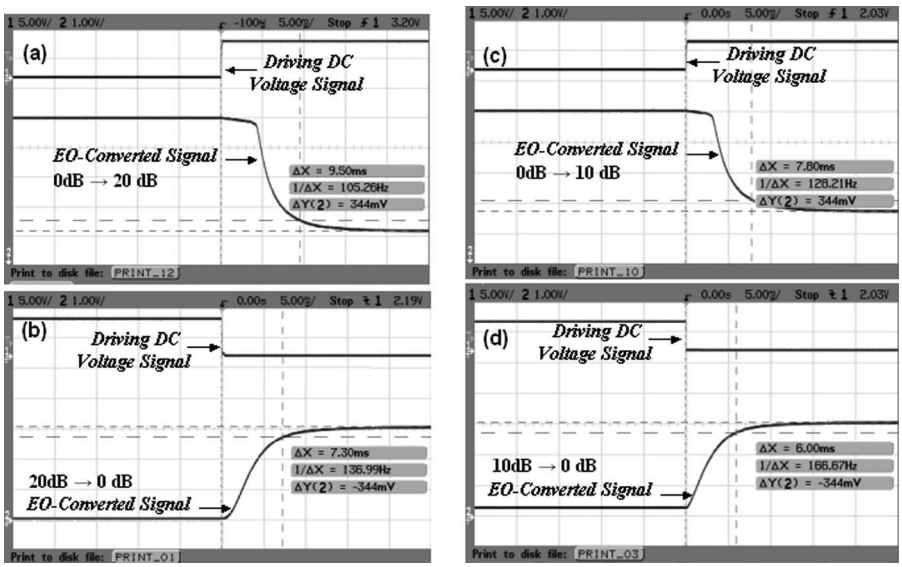

Fig. 7. Switching time between states of (a) and (b) zero attenuation and attenuation of 20 dB and (c) and (d) zero attenuation and attenuation of 10 dB.

will be a concern and crucial to practical VOA applications. In fact, the measured data discussed in the previous section have revealed very good stability and repeatability of attenuation characteristics versus driving voltage at 0 °C, 25 °C, and 75 °C, but it is still suspicious that the surrounding temperature of the VOA device during operation, i.e., the ambient temperature, may influence the displacement versus driving voltage characteristics in terms of the difference in heat dissipation rate of the electrothermal actuators. As a result, an additional experiment was carried out for this purpose, because such an effect may introduce the deviated characteristics of attenuation versus driving voltage when the ambient temperature varies. The VOA device was kept in a temperature-controlled chamber. Then, the attenuation versus driving voltage curves were measured at 25 °C first and then measured again at 75 °C when the chamber temperature is elevated up to 75 °C. The derived curves are shown in Fig. 6(a). Basically, the revealed difference in attenuation for these two curves is limited, and it is between $+0.1$ and -0.4 dB within the 40-dB attenuation range. On the other hand, Fig. 6(b) and (c) shows the measured difference of attenuation curves measured under the same procedures of 25 °C to 12.5 °C and 25 °C to 0 °C, respectively. Within the 40-dB attenuation range, the revealed difference of attenuation is varied in the range of 0 to -0.6 dB for the case of 25 °C to 12.5 °C in Fig. 6(b), while this difference is increased and becomes in the range of 0 to -1.3 dB for the case of 25 °C to 0 °C in Fig. 6(c), which is a reasonable result. Since the rate of heat dissipation from the actuated and heated H-shaped beam structure to the environment becomes larger due to the larger temperature difference in the case of 0 °C ambient temperature, more driving voltage is required to reach the same attenuation value, where the driving electrical power is in proportion to this driving voltage. Therefore, the attenuation curve measured at 0 °C ambient temperature is shifted to the right-hand side of the high-driving voltage region. A new kind of package with a better thermal isolation characteristic may reduce this sort of influence. It could be further characterized in the future.

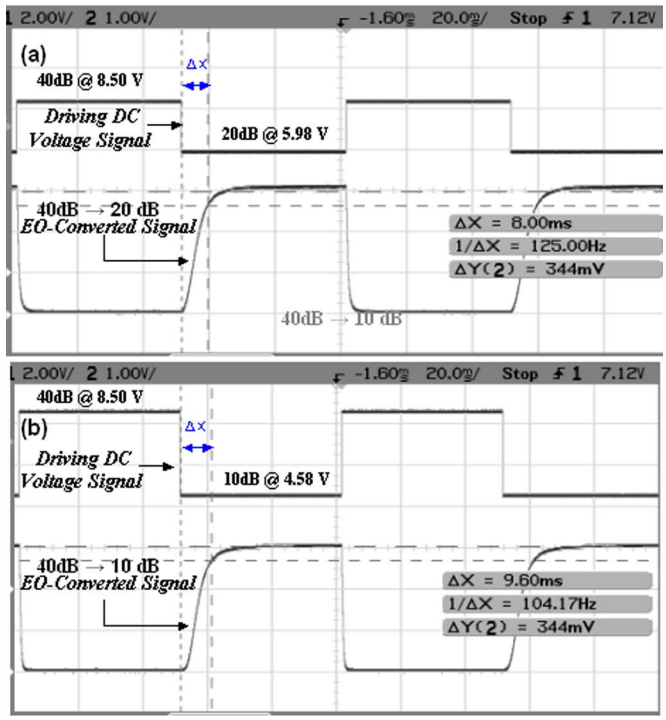

Fig. 8. Switching time between states of (a) 40-dB attenuation to 20-dB attenuation and (b) switching time between states of 40-dB attenuation to 10-dB attenuation.

The switching speed between two attenuation states is an important parameter that is considered by most applications. For particular VOA devices with known attenuation versus driving voltage curve, the 1550-nm optical signals are provided from the input port to the device under test, and then, the received optical power from the output is converted into voltage signals via an opto–electro converter. The signals measured in this transient procedure between two attenuation states were recorded by an oscilloscope. Fig. 7(a) and (b) shows the measured switching speed data for switching between 0- and 20-dB

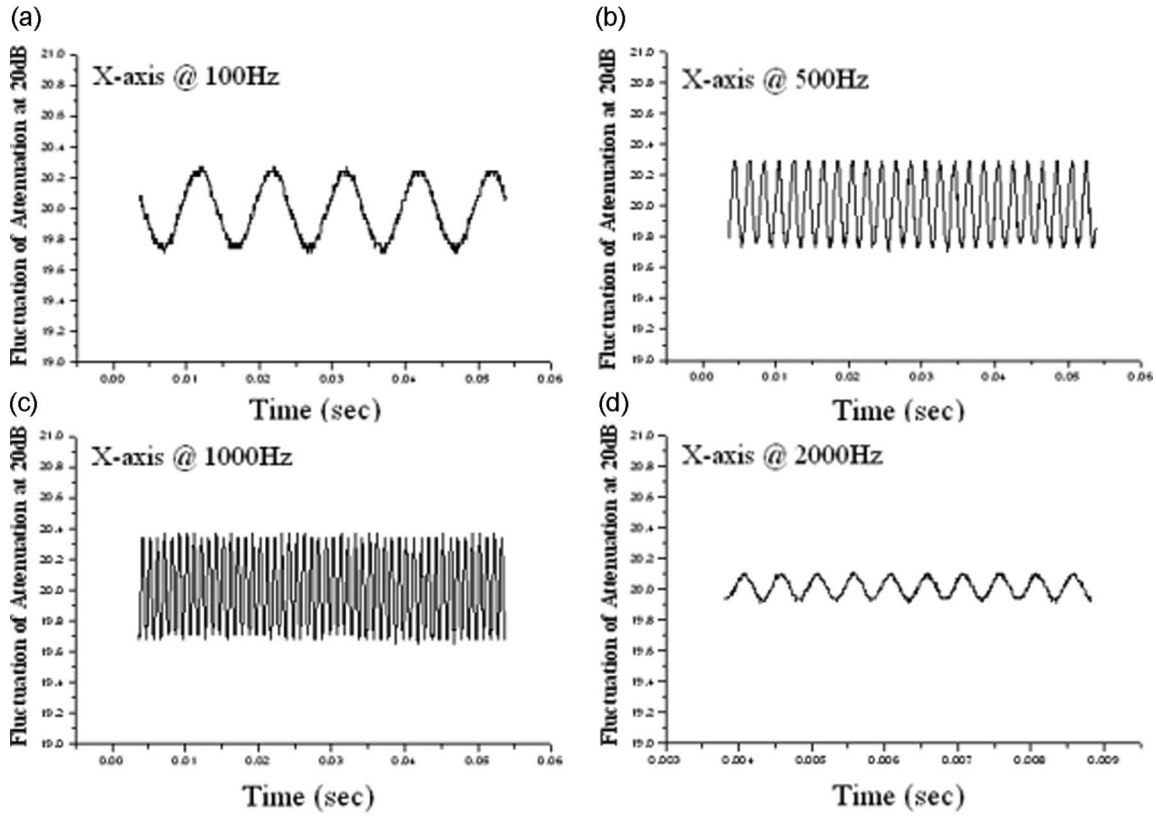

Fig. 9. Measured fluctuated attenuation value of 20-dB attenuation for an H-shaped MEMS VOA under a mechanical vibration of 20 G along the x-axis, i.e., mirror-moving axis at (a) 100 Hz, (b) 500 Hz, (c) 1 kHz, and (d) 2 kHz.

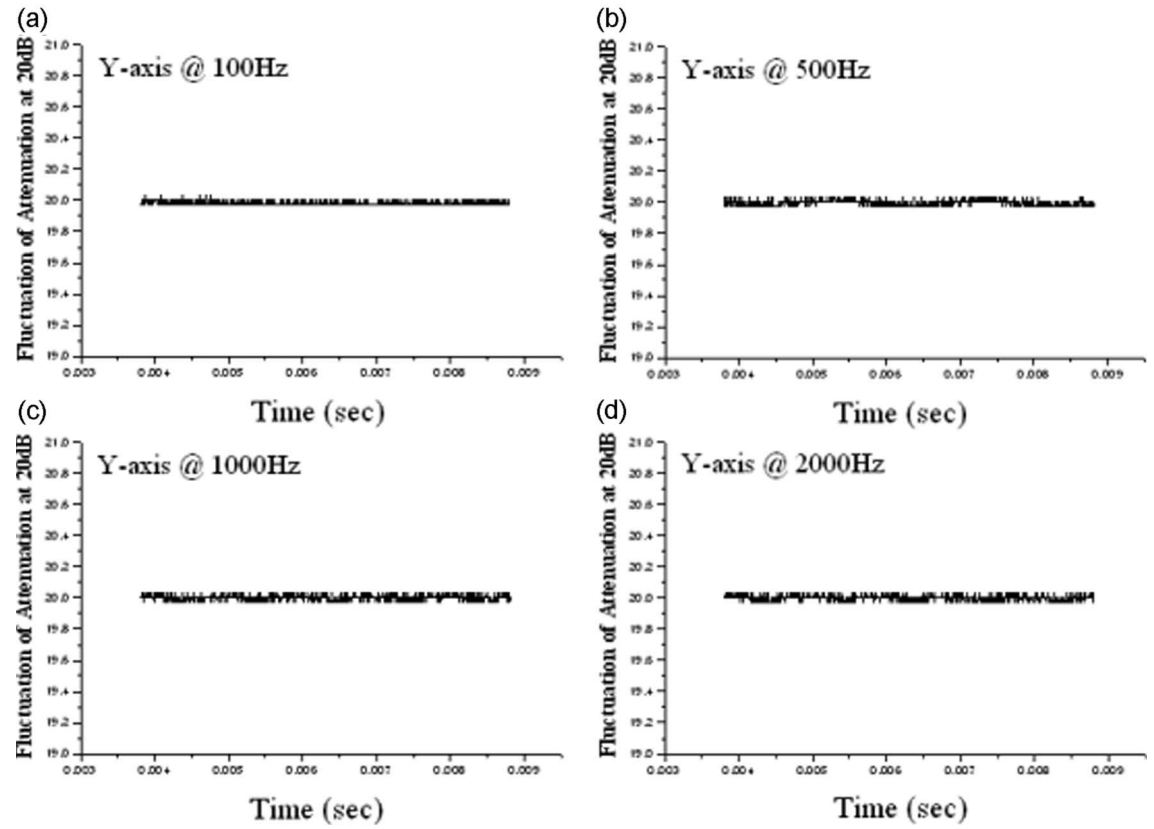

Fig. 10. Measured fluctuated attenuation value of 20-dB attenuation for an H-shaped MEMS VOA under a mechanical vibration of 20 G along the y-axis, i.e., planar perpendicular direction with regard to the mirror-moving axis at (a) 100 Hz, (b) 500 Hz, (c) 1 kHz, and (d) 2 kHz.

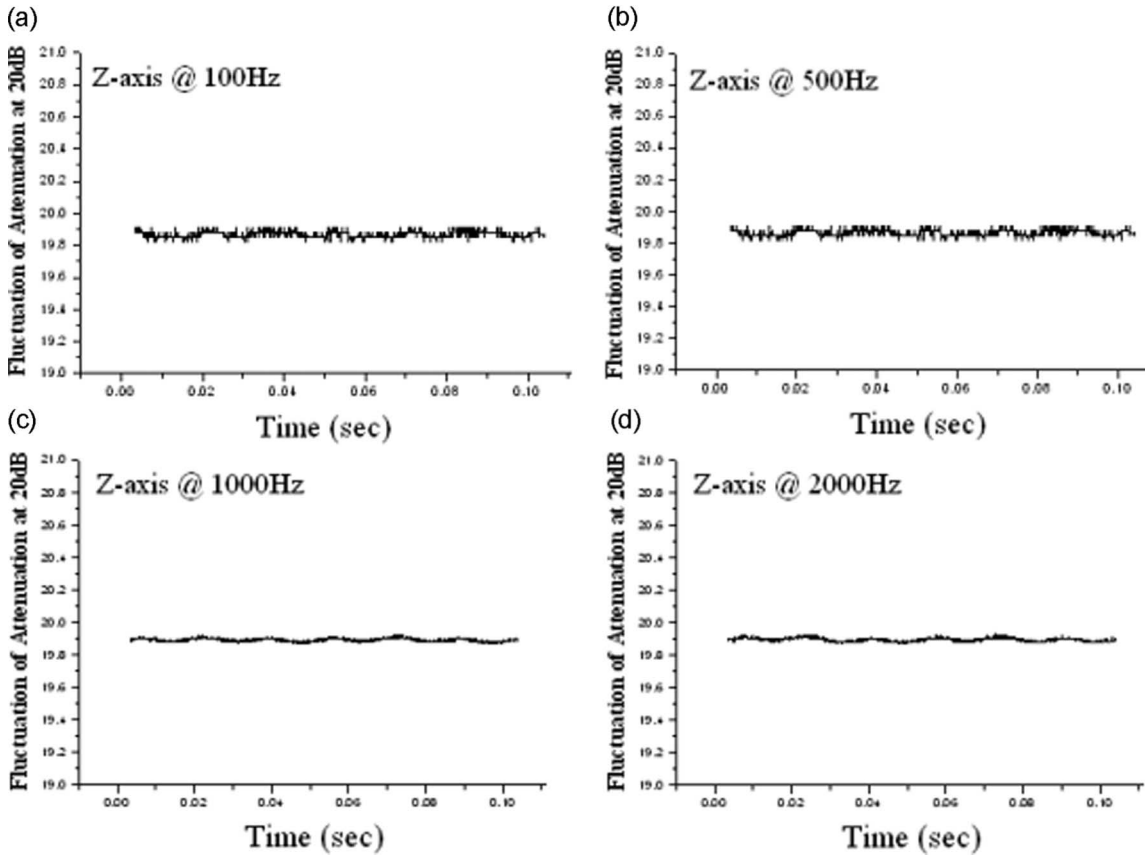

Fig. 11. Measured fluctuated attenuation value of 20-dB attenuation for an H-shaped MEMS VOA under a mechanical vibration of 20 G along the z-axis, i.e., out-of-plane perpendicular direction with regard to the mirror-moving axis at (a) 100 Hz, (b) 500 Hz, (c) 1 kHz, and (d) 2 kHz.

attenuation, respectively, when the device was biased by 5.98 V dc. This requires 9.5 ms for the actuator to move mirrors from positions of 0 to 20 dB and 7.3 ms for the reversed step. Besides, Fig. 7(c) and (d) shows the measured data for switching between 0- and 10-dB attenuation under 4.58 V dc bias, respectively, which reveals that 7.8 and 6 ms are measured for the triggering device from nonattenuation state to 10-dB attenuation state and returning this device back to its rest state, respectively. Based on the data shown in Fig. 7, the reason for 9.5 ms being longer than 7.8 ms is because the H-shaped structure has to be deformed more in order to generate a larger displacement for mirrors with regard to a larger attenuation value. The switching-back step is faster than the switching-on step for all the measured data. The switching-back time should be determined by the lead time of releasing the joule heat from the H-shaped beam structure after removing the electrical bias. In other words, the deformed H-shaped beam structure will return to its initial shape and drive the mirrors back to their rest position when the electrical bias is removed. This fact may be attributed to the potential reason that this lead time is shorter than the overall switching-on time, including the time period required for the rising temperature of the H-shaped beam structure to generate the initial movement and the time period of moving mirrors from their initial position to the position of the corresponding attenuation.

Fig. 8(a) and (b) shows the measured data for switching between two attenuation states of 40–20 and 40–10 dB, respectively. Again, the switching time for 40–10 dB is measured as 9.6 ms and is longer than the 8 ms for the case of switching from 40 to 20 dB. It could just be simply concluded as the mirror-moving displacement for the case of 40–10 dB is longer than the case of 40–20 dB. Fortunately, all the measured data for switching among various attenuation states within the 40-dB attenuation region are less than 10 ms. The switching time of 10 ms is acceptable for most industrial applications.

In addition to the above experiments, which were mainly focused on the study of the nature of electrothermal actuation for VOA applications, the device characteristics regarding the Telecordia GR1221 regulation are very interesting for practical applications. Based on this Telecordia GR1221 regulation, we conducted mechanical shock testing with the condition of five shocks of 500 G along with six directions for 1-ms impact duration. The optical characteristics of devices after this testing were measured again and compared with their previous data. Basically, all data measured after the shock test exhibit the same quality of performance as the data measured before this experiment. It is worthy to address again that the anti-shock stopper structure has successfully avoided the overshoot-like movement along with the moving axis of the structure, i.e., the x-axis, to protect the MEMS VOA structure.

GR1221 also requests that the dynamic deviation value at 20-dB attenuation should be less than ± 0.5 dB under a vibration testing condition of 20 G periodical shocks with frequency from 20 Hz to 2 kHz along the x-, y-, and z-axes, where

four cycles of vibrations are required for each axis. Fig. 9 shows the data for 20 G periodical shocks introduced along the x-axis, where the x-axis is the most compliant axis, as shown in Fig. 2(a). It is observed that the measured attenuation fluctuation data are less than ± 0.28, ± 0.3, ± 0.36, and ± 0.1 dB for a frequency of 20 G periodical shocks maintained at 100 Hz, 500 Hz, 1 kHz, and 2 kHz, respectively. Besides, Figs. 10 and 11 show the measured data for 20 G periodical shocks introduced along the y- and z-axes, where the y- and z-axes are the planar perpendicular direction and the out-of-plane perpendicular direction to the x-axis, respectively, as shown in Fig. 2(a). Relatively stable dynamic characteristics are shown in Figs. 10 and 11, which reveals that the measured fluctuation is less than ± 0.03 and ± 0.15 dB over the full range with regard to the y- and z-axes, since the nature of the symmetric H-shaped beam structure of the VOA device with four anchors on corners and the high aspect ratio of the side beam along the z-direction provide excellent mechanical stability against mechanical vibrations. The above results of the dynamic attenuation characteristics prove that the present device complies with the Telecordia GR1221 regulations.

IV. Conclusion

This paper provides the first insight study on the correlation among the mechanics and optical characteristics of MEMS VOAs using an H-shaped structure. While most of the MEMS VOA alternatives up until now are based on electrostatic approaches, H-shaped electrothermal actuators are adopted to enable a retroreflection-type MEMS VOA of smaller footprint. The voltage and driving power for 30 and 50 dB are measured as 8.1 V and 135 mW and 10.2 V and 210 mW, respectively. The deviation of attenuation curves under the same driving voltage and the same ambient temperatures is less than ± 0.1 dB. Additionally, the deviation of attenuation curves for comparison made for 25 °C to 75 °C and for 25 °C to 12.5 °C is characterized as within the 0.6-dB range. Switching time requires 10 ms or less for all cases of switching between two attenuation states and from nonattenuation state to a particular attenuation state within the 40-dB attenuation range. This new MEMS VOA also demonstrates the state-of-the-art dynamic attenuation stability that complies with the Telecordia GR1221 regulations, where the dynamic deviation value of attenuation at 20 dB is less than ± 0.36 dB under a vibration testing condition of 20 G periodical shocks with frequency from 20 Hz to 2 kHz. The simple and symmetric shape of this MEMS VOA device structure contributes to the outstanding dynamic attenuation stability. The current results prove that using electrothermal actuators should be one good alternative for driving MEMS VOAs. It confirms its potential for commercial applications.

Acknowledgment

The author would like to thank Asia Pacific Microsystems, Inc. for the support and effort related to packaging and reliability test.

References

[1] L. Y. Lin and E. L. Goldstein, "Opportunities and challenges for MEMS in lightwave communications," *IEEE J. Sel. Topics Quantum Electron.*, vol. 8, no. 1, pp. 163–172, Jan./Feb. 2002.

[2] J. E. Ford, K. W. Goossen, J. A. Walker, D. T. Neilson, D. M. Tennant, S. Y. Park, and J. W. Sulhoff, "Interference-based micromechanical spectral equalizers," *IEEE J. Sel. Topics Quantum Electron.*, vol. 10, no. 3, pp. 579–587, May/Jun. 2004.

[3] M. Yano, F. Yamagishi, and T. Tsuda, "Optical MEMS for photonic switching—Compact and stable optical crossconnect switches for simple, fast, and flexible wavelength applications in recent photonic networks," *IEEE J. Sel. Topics Quantum Electron.*, vol. 11, no. 2, pp. 383–394, Mar./Apr. 2005.

[4] B. Barber, C. R. Giles, V. Askyuk, R. Ruel, L. Stulz, and D. Bishop, "A fiber connectorized MEMS variable optical attenuator," *IEEE Photon. Technol. Lett.*, vol. 10, no. 9, pp. 1262–1264, Sep. 1998.

[5] J. E. Ford and J. A. Walker, "Dynamic spectral power equalization using micro-opto-mechanics," *IEEE Photon. Technol. Lett.*, vol. 10, no. 10, pp. 1440–1442, Oct. 1998.

[6] X. M. Zhang, A. Q. Liu, C. Lu, and D. Y. Tang, "MEMS variable optical attenuator using low driving voltage for DWDM systems," *Electron. Lett.*, vol. 38, no. 8, pp. 382–383, Apr. 2002.

[7] A. Q. Liu, X. M. Zhang, C. Lu, F. Wang, C. Lu, and Z. S. Liu, "Optical and mechanical models for a variable optical attenuator using a micromirror drawbridge," *J. Micromech. Microeng.*, vol. 13, no. 3, pp. 400–411, May 2003.

[8] X. M. Zhang, A. Q. Liu, C. Lu, F. Wang, and Z. S. Liu, "Polysilicon micromachined fiber-optical attenuator for DWDM applications," *Sens. Actuators A, Phys.*, vol. 108, no. 1–3, pp. 28–35, Nov. 2003.

[9] K. Isamoto, K. Kato, A. Morosawa, C. Chong, H. Fujita, and H. Toshiyoshi, "A 5-V operated MEMS variable optical attenuator by SOI bulk micromachining," *IEEE J. Sel. Topics Quantum Electron.*, vol. 10, no. 3, pp. 570–578, May/Jun. 2004.

[10] C. Marxer, P. Griss, and N. F. de Rooij, "A variable optical attenuator based on silicon micromechanics," *IEEE Photon. Technol. Lett.*, vol. 11, no. 2, pp. 233–235, Feb. 1999.

[11] C. Chen, C. Lee, Y.-J. Lai, and W.-C. Chen, "Development and application of lateral comb drive actuator," *Jpn. J. Appl. Phys. 1, Regul. Rap. Short Notes*, vol. 42, no. 6B, pp. 4067–4073, Jun. 2003.

[12] C. Chen, C. Lee, and Y.-J. Lai, "Novel VOA using in-plane reflective micromirror and off-axis light attenuation," *IEEE Commun. Mag.*, vol. 41, no. 8, pp. S16–S20, Aug. 2003.

[13] Y. Y. Kim, S. S. Yun, C. S. Park, J.-H. Lee, Y. G. Lee, H. K. Lee, S. K. Yoon, and J. S. Kang, "Refractive variable optical attenuator fabricated by silicon deep reactive ion etching," *IEEE Photon. Technol. Lett.*, vol. 16, no. 2, pp. 485–487, Feb. 2004.

[14] A. Bashir, P. Katila, N. Ogier, B. Saadany, and D. A. Khalil, "A MEMS-based VOA with very low PDL," *IEEE Photon. Technol. Lett.*, vol. 16, no. 4, pp. 1047–1049, Apr. 2004.

[15] C. Chen, C. Lee, and J. A. Yeh, "Retro-reflection type MOEMS VOA," *IEEE Photon. Technol. Lett.*, vol. 16, no. 10, pp. 2290–2292, Oct. 2004.

[16] H. Cai, X. M. Zhang, C. Lu, A. Q. Liu, and E. H. Khoo, "Linear MEMS variable optical attenuator using reflective elliptical mirror," *IEEE Photon. Technol. Lett.*, vol. 17, no. 2, pp. 402–404, Feb. 2005.

[17] C.-H. Kim and Y.-K. Kim, "MEMS variable optical attenuator using translation motion of 45° tilted vertical mirror," *J. Micromech. Microeng.*, vol. 15, no. 8, pp. 1466–1475, Aug. 2005.

[18] T.-S. Lim, C.-H. Ji, C.-H. Oh, H. Kwon, Y. Yee, and J. U. Bu, "Electrostatic MEMS variable optical attenuator with rotating folded micromirror," *IEEE J. Sel. Topics Quantum Electron.*, vol. 10, no. 3, pp. 558–562, May/Jun. 2004.

[19] J. A. Yeh, S.-S. Jiang and C. Lee, "MOEMS VOA using rotary comb drive actuators," *IEEE Photon. Technol. Lett.*, to be published.

[20] C. Lee and Y.-S. Lin, "A new micromechanism for transformation of small displacements to large rotations for a VOA," *IEEE Sensors J.*, vol. 4, no. 4, pp. 503–509, Aug. 2004.

[21] J. C. Chiou and W. T. Lin, "Variable optical attenuator using a thermal actuator array with dual shutters," *Opt. Commun.*, vol. 237, no. 4–6, pp. 341–350, Jul. 2004.

[22] R. R. A. Syms, H. Zou, J. Stagg, and H. Veladi, "Sliding-blade MEMS iris and variable optical attenuator," *J. Micromech. Microeng.*, vol. 14, no. 12, pp. 1700–1710, Dec. 2004.

[23] C. Lee, "Variable optical attenuator using planar light attenuation scheme based on rotational and translational misalignment," *Microsyst. Technol.*, vol. 13, no. 1, pp. 41–48, Oct. 2005.

[24] ——, "MOEMS variable optical attenuator with improved dynamic characteristics based on robust design," *IEEE Photon. Technol. Lett.*, vol. 18, no. 6, pp. 773–775, Mar. 2006.
[25] ——, "Monolithic-integrated 8CH MEMS variable optical attenuators," *Sens. Actuators A, Phys.*, vol. 123/124, pp. 596–601, Sep. 2005.
[26] ——, "Arrayed variable optical attenuator using retro-reflective MEMS mirrors," *IEEE Photon. Technol. Lett.*, vol. 17, no. 12, pp. 2640–2642, Dec. 2005.
[27] G. Wu, A. R. Mirza, S. K. Gamage, L. Ukrainczyk, N. Shashidhar, G. Wruck, and M. Ruda, "Design and use of compact lensed fibers for low cost packaging of optical MEMS components," *J. Micromech. Microeng.*, vol. 14, no. 10, pp. 1367–1375, Oct. 2004.
[28] C. Lee and C.-Y. Wu, "Study of electrothermal V-beam actuators and latched mechanism for optical switch," *J. Micromech. Microeng.*, vol. 15, no. 1, pp. 11–19, Jan. 2005.
[29] W.-C. Chen, C. Lee, C.-Y. Wu, and W. Fang, "A new latched 2×2 optical switch using bi-directional movable electrothermal H-beam actuators," *Sens. Actuators A, Phys.*, vol. 123/124, pp. 563–569, Sep. 2005.

Chengkuo Lee (S'94–M'96) received the M.S. degree in materials science and engineering from the National Tsing Hua University, Hsinchu, Taiwan, R.O.C., in 1991, the M.S. degree in industrial and system engineering from Rutgers University, New Brunswick, NJ, in 1993, and the Ph.D. degree in precision engineering from the University of Tokyo, Tokyo, Japan, in January 1996.

From 1993 to 1996, he was a Foreign Researcher with the Nanometer-Scale Manufacturing Science Laboratory, Research Center for Advanced Science and Technology (RCAST), University of Tokyo. In 1996, he was with the Mechanical Engineering Laboratory, AIST, MITI, Japan, as a JST Research Fellow. Thereafter, he was a Senior Research Staff with Microsystems Laboratory, Industrial Technology Research Institute (ITRI), Hsinchu. Since September 1997, he has been with the Metrodyne Microsystem Corporation, Hsinchu, where he established the MEMS device division and the first micromachining fabrication for commercial purposes in Taiwan and was the Manager of the MEMS Device Division between 1997 and 2000. He was also an Adjunct Assistant Professor with the Electro-Physics Department, National Chiao Tung University, Hsinchu, in 1998, and an Adjunct Assistant Professor with the Institute of Precision Engineering, National Chung Hsing University, Taichung, Taiwan, from 2001 to 2005. He cofounded Asia Pacific Microsystems, Inc. (APM), Hsinchu, in August 2001 and was the Vice-President of R&D before becoming the VP of the Optical Communication Business Unit and Special Assistant to the CEO, in charge of international business and technical marketing for MEMS foundry service at APM, Inc., until the end of 2005. APM achieved annual revenue of US$13M in 2005 and was ranked in the top 30 in the world for MEMS manufacturers in 2004. He is currently an Assistant Professor with the Department of Electrical and Computer Engineering, National University of Singapore, Singapore, and a Senior Member of Technical Staff with the Institute of Microelectronics (IME), A*Star, Singapore. He has contributed more than 70 international conference papers and extended abstracts, 40 peer-reviewed international journal articles, and eight U.S. patents in the MEMS and nanotechnology field.

Dr. Lee is a member of MRS and IEE Japan.